

## **ANALYSIS OF REWETTING OF AN INFINITE TUBE BY NUMERICAL FOURIER INVERSION**

A.K. Satapathy and R.K. Sahoo  
Department of Mechanical Engineering  
Regional Engineering College  
ROURKELA-769 008  
Orissa, INDIA

A semi-analytical model for the two-dimensional quasi-steady conduction equation, governing conduction controlled rewetting of an infinite tube, has been suggested. The solution yields the temperature field as a function of various input model parameters such as Peclet number, Biot number and radius ratio of the tube. Unlike earlier investigations, the present semi-analytical model predicts the temperature field for the entire domain of a tube, employing the Wiener-Hopf technique and by inverse discrete Fourier transform (IDFT) algorithm.

© 2002 Elsevier Science Ltd

### **Introduction**

The process of rewetting of hot surfaces is of practical importance in nuclear and metallurgical industries. For instance, in a postulated loss-of-coolant accident (LOCA) of a nuclear reactor, the overheated rod clusters are cooled down by the emergency core cooling water which are introduced into the core in the form of either top spray or bottom flooding. However, the injected coolant does not immediately wet the cladding surface because a stable vapor blanket would prevent the liquid-solid contact. The maximum surface temperature at which the coolant establishes contact with the hot surface is the rewetting or quench front temperature. When the cladding surface is below the quench front temperature, rewetting occurs. The upstream end of the solid (wet region) is cooled by convection to the contacting liquid, while its downstream (dry region) is cooled by heat transfer to a mixture of vapor and liquid droplets (precursory cooling).

The rewetting model for a two-dimensional two-region heat transfer with a step change in heat transfer coefficient at the quench front has been solved for a single slab [1–3], for a composite slab [4], for a single rod [5] and for a composite cylinder [6]. In the single tube/slab model the dryside is considered to be adiabatic, whereas in case of a composite tube/slab model a three layer composite is considered to simulate the fuel and the cladding separated by a gas filled gap between them. The rewetting model in a plate geometry with a uniform boundary heat flux has been solved by Chan and Zhang [7]. The solution methods commonly employed are either separation of variables or Wiener–Hopf technique and the solutions have been obtained for either quench front temperature or quench front velocity. Reported literature on analytical investigations of rewetting indicates that Wiener–Hopf solution for various rewetting models has been obtained only for the quench front temperature. In the present analysis, however, a semi-analytical model has been suggested so as to obtain the temperature distribution in the entire physical domain, by numerical Fourier inversion.

In the present study, the physical system consists of an infinitely extended vertical tube with outer surface flooded and the inside surface insulated. The model assumes a constant heat transfer coefficient for the wet region while the dry region is assumed to be adiabatic. The solution procedure proposed herewith generally consists of two steps: first, the governing equation with its associated boundary conditions is solved in a complex Fourier plane employing the Wiener–Hopf technique. Second, the temperature solution so obtained is then inverted back to its physical plane by using the IDFT algorithm.

### **Mathematical Model**

The two-dimensional transient heat conduction equation for the tube (Fig.1) is

$$\frac{1}{R} \frac{\partial}{\partial R} \left( R \frac{\partial T}{\partial R} \right) + \frac{\partial^2 T}{\partial Z^2} = \frac{\rho C}{k} \frac{\partial T}{\partial t} \quad R_1 < R < R_2 \quad 0 < Z < L \quad L \rightarrow \infty \quad (1)$$

where  $L$  is the length of the tube and  $R_1$ ,  $R_2$  are inner and outer radius of the tube. The density, specific heat and thermal conductivity of the tube material are  $\rho$ ,  $C$  and  $k$  respectively. The origin of the coordinate frame is at the bottom point on the axis of the tube. To convert this transient equation into a quasi-steady state equation, the following moving coordinate system is used:

$$\bar{R} = R \quad \bar{Z} = Z - ut$$

where  $u$  is the constant quench front velocity and  $\bar{R}$  and  $\bar{Z}$  are radial and axial coordinates respectively (Fig.1). Thus the quasi-steady heat conduction equation in a coordinate system moving with the quench front is

$$\frac{1}{\bar{R}} \frac{\partial}{\partial \bar{R}} \left( \bar{R} \frac{\partial T}{\partial \bar{R}} \right) + \frac{\partial^2 T}{\partial \bar{Z}^2} + \frac{\rho C u}{k} \frac{\partial T}{\partial \bar{Z}} = 0 \quad R_1 < \bar{R} < R_2 \quad -\infty < \bar{Z} < \infty \quad (2)$$

In the present analysis, the heat transfer coefficient  $h$  is assumed to be constant over the entire wet region. The dry region and inner core of the tube are assumed to be adiabatic. The coolant temperature is taken to be equal to its saturation temperature  $T_s$ . Moreover, it is assumed that at far upstream of the quench front (at  $\bar{Z} \rightarrow -\infty$ ), the tube has been quenched to a temperature  $T_s$ , while the far pre-quenched zone (at  $\bar{Z} \rightarrow +\infty$ ) is still at its initial temperature  $T_w$ . The following non-dimensional variables are then introduced.

$$r = \frac{\bar{R}}{R_2}, \quad z = \frac{\bar{Z}}{R_2}, \quad \theta = \frac{T - T_s}{T_w - T_s}, \quad Bi = \frac{hR_2}{k}, \quad Pe = \frac{\rho C u R_2}{k}, \quad \delta = \frac{R_1}{R_2} \quad (3)$$

Equation (2) can be expressed in the following dimensionless form

$$\frac{1}{r} \frac{\partial}{\partial r} \left( r \frac{\partial \theta}{\partial r} \right) + \frac{\partial^2 \theta}{\partial z^2} + Pe \frac{\partial \theta}{\partial z} = 0 \quad \delta < r < 1 \quad -\infty < z < \infty \quad (4)$$

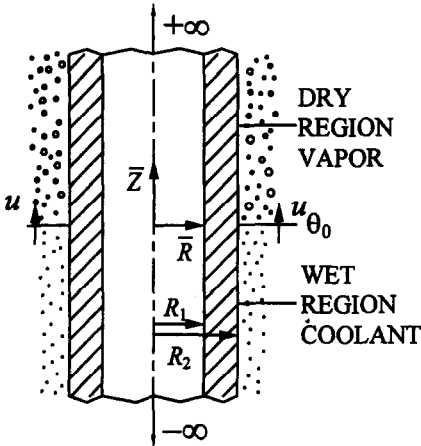


FIG.1  
Physical domain of the infinite tube.

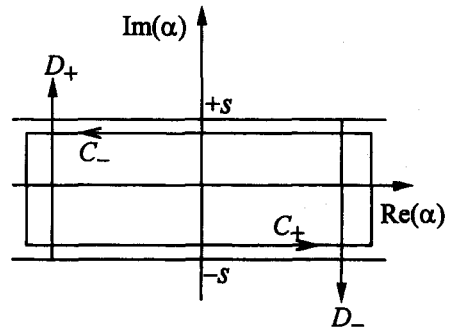


FIG.2  
Common strip of analyticity in the complex Fourier plane.

The associated boundary conditions are

$$\begin{aligned}
 \frac{\partial \theta}{\partial r} = 0 & \quad \text{at} \quad r = \delta & \quad -\infty < z < \infty \\
 \frac{\partial \theta}{\partial r} + Bi\theta = 0 & \quad \text{at} \quad r = 1 & \quad z < 0 \\
 \frac{\partial \theta}{\partial r} = 0 & \quad \text{at} \quad r = 1 & \quad z > 0 \\
 \theta = 0 & \quad \text{at} \quad z \rightarrow -\infty \\
 \theta = 1 & \quad \text{at} \quad z \rightarrow +\infty
 \end{aligned} \tag{5}$$

The non-dimensional quench front temperature defined by  $\theta_0 = (T_0 - T_s) / (T_w - T_s) = \theta(1,0)$ , in which,  $T_0$  is the quench front temperature. The main objective of the present study is to compute the quench front temperature  $\theta_0$  in terms of various input model parameters, namely, Biot number  $Bi$ , Peclet number  $Pe$  and radius ratio  $\delta$ . Also, the temperature distribution elsewhere in the tube has been obtained by numerical Fourier inversion, for the prescribed values of above model parameters.

### Analytical Solution

In order to employ the Wiener-Hopf technique, Eq.(4) is first transformed with a new dependent variable  $\varphi$ , defined by  $\theta(r,z) = 1 - \varphi(r,z)e^{-sz}$ , in which  $s=Pe/2$ . The governing equation (Eq.(4)) then becomes

$$\frac{1}{r} \frac{\partial}{\partial r} \left( r \frac{\partial \varphi}{\partial r} \right) + \frac{\partial^2 \varphi}{\partial z^2} - s^2 \varphi = 0 \quad \delta < r < 1 \quad -\infty < z < \infty \tag{6}$$

The boundary conditions in Eq.(5) can be written sequentially as:

$$\begin{aligned}
 \frac{\partial \varphi}{\partial r} = 0 & \quad \text{at} \quad r = \delta & \quad -\infty < z < \infty \\
 \frac{\partial \varphi}{\partial r} + Bi\varphi = Bie^{sz} & \quad \text{at} \quad r = 1 & \quad z < 0 \\
 \frac{\partial \varphi}{\partial r} = 0 & \quad \text{at} \quad r = 1 & \quad z > 0 \\
 \varphi = e^{sz} & \quad \text{at} \quad z \rightarrow -\infty \\
 \varphi = 0 & \quad \text{at} \quad z \rightarrow +\infty
 \end{aligned} \tag{7}$$

In the next step of the present analysis, Fourier transform is used to convert the partial differential equation (Eq.(6)) to an ordinary differential equation. The Fourier transform is defined by

$$\Phi(\alpha, r) = \Phi_+(\alpha, r) + \Phi_-(\alpha, r) = \int_{-\infty}^{\infty} \varphi(r, z) e^{i\alpha z} dz \quad (8)$$

with  $\Phi_-(\alpha, r) = \int_{-\infty}^0 \varphi(r, z) e^{i\alpha z} dz$  and  $\Phi_+(\alpha, r) = \int_0^{\infty} \varphi(r, z) e^{i\alpha z} dz$ . The parameter  $\alpha$  used above is

a complex quantity. The far-field boundary conditions in Eq.(7) indicate that  $\varphi(r, z)$  is of the order  $\exp(sz)$  at  $z \rightarrow -\infty$ , whereas  $\varphi(r, z)$  is of the order  $\exp(-sz)$  at  $z \rightarrow +\infty$ . The above two conditions ensure that the functions  $\Phi_+(\alpha, r)$  and  $\Phi_-(\alpha, r)$  are analytic in the domains  $D_+$  and  $D_-$  respectively. The domains  $D_+$  and  $D_-$  are defined (Fig.2) in the entire complex domain as:

$$D_+ : \text{Im}(\alpha) > -s \quad \text{and} \quad D_- : \text{Im}(\alpha) < +s.$$

Applying the Fourier transform, Eq.(6) assumes the form

$$\frac{1}{r} \frac{\partial}{\partial r} \left( r \frac{\partial \Phi}{\partial r} \right) - \gamma^2 \Phi = 0 \quad (9)$$

in which  $\gamma = (\alpha^2 + s^2)^{1/2}$ . The transformed boundary conditions are

$$\Phi'(\alpha, \delta) = 0$$

$$\Phi'_-(\alpha, 1) + Bi\Phi_-(\alpha, 1) = -\frac{i}{\alpha - is} Bi$$

$$\Phi'_+(\alpha, 1) = 0 \quad (10)$$

where prime denotes the transform of  $r$ -derivatives of  $\varphi(r, z)$ . The general solution of the second order ordinary differential equation (Eq.(9)) is

$$\Phi(\alpha, r) = C_1(\alpha) I_0(\gamma r) + C_2(\alpha) K_0(\gamma r) \quad (11)$$

where  $I_0, K_0$  are zeroth-order modified Bessel functions of first and second kinds respectively.

Imposing the boundary conditions of Eq.(10) into Eq.(11) yields

$$\Phi_+(\alpha, 1) + \left[ 1 + \frac{Bi}{\gamma f(\gamma)} \right] \Phi_-(\alpha, 1) = -\frac{i}{\alpha - is} \left[ \frac{Bi}{\gamma f(\gamma)} \right] \quad (12)$$

where  $f(\gamma) = \frac{I_1(\gamma)K_1(\gamma\delta) - I_1(\gamma\delta)K_1(\gamma)}{I_0(\gamma)K_1(\gamma\delta) + I_1(\gamma\delta)K_0(\gamma)}$  and  $I_1, K_1$  are first-order modified Bessel functions

of first and second kinds respectively. The key step in successful implementation of Wiener-Hopf

technique depends on factorization of a function, which is analytic in a strip, into the product of two functions that are analytic in the overlapping half-planes ( $D_+$  and  $D_-$ ). In this regard, let

$$K(\alpha) = K_+(\alpha) K_-(\alpha) = 1 + \frac{Bi}{\gamma f(\gamma)} \quad (13)$$

where the functions  $K_+(\alpha)$ ,  $K_-(\alpha)$  are analytic in the domains  $D_+$  and  $D_-$  respectively. Now the kernel function  $K(\alpha)$ , in connection with Eq.(12), is to be decomposed to  $K_+(\alpha)$  and  $K_-(\alpha)$  in accordance with Wiener–Hopf technique. This is accomplished by rearranging Eq.(12) to obtain

$$\frac{\Phi_+(\alpha,1)}{K_+(\alpha)} - \frac{i}{\alpha - is} \left[ \frac{1}{K_+(\alpha)} - \frac{1}{K_+(is)} \right] = -\Phi_-(\alpha,1)K_-(\alpha) - \frac{i}{\alpha - is} \left[ K_-(\alpha) - \frac{1}{K_+(is)} \right] \quad (14)$$

In Eq.(14), each side characterizes the same ‘entire function’, through its representation in the upper and lower halves of the  $\alpha$ -plane. Since  $\Phi_+(\alpha,1)$  and  $\Phi_-(\alpha,1)$  tend to zero at infinity in their half-planes of analyticity, while  $K_+(\alpha)$  and  $K_-(\alpha)$  remain bounded, it turns out that the entire function vanishes according to Liouville’s theorem. Hence, equating both sides of the Eq.(14) to zero,  $\Phi_+(\alpha,1)$  and  $\Phi_-(\alpha,1)$  are determined as

$$\Phi_+(\alpha,1) = \frac{i}{\alpha - is} \left[ 1 - \frac{K_+(\alpha)}{K_+(is)} \right], \quad \Phi_-(\alpha,1) = -\frac{i}{\alpha - is} \left[ 1 - \frac{1}{K_-(\alpha)K_+(is)} \right] \quad (15)$$

The temperature distribution in the tube can be obtained by the inversion relation

$$\theta(r,z) = 1 - \frac{e^{-sz}}{2\pi} \int_{-\infty}^{+\infty} \Phi(\alpha,1)g(\gamma)e^{-i\alpha z} d\alpha \quad (16)$$

in which,  $g(\gamma) = \frac{I_0(\gamma r)K_1(\gamma\delta) + I_1(\gamma\delta)K_0(\gamma r)}{I_0(\gamma)K_1(\gamma\delta) + I_1(\gamma\delta)K_0(\gamma)}$ . Using the expressions of  $\Phi_+(\alpha,1)$  and  $\Phi_-(\alpha,1)$ ,

as specified in Eq.(15), the temperature field may be obtained by inverting its Fourier transform (Eq.(16)) analytically. Such an attempt may become tedious because, in order to perform the Fourier inversion, it would be necessary to evaluate the residues of  $\Phi(\alpha,1)$  function in its complex  $\alpha$ -plane. Alternatively, in the present paper this inversion has been carried out numerically by employing the IDFT algorithm. In this regard, let  $\alpha = \omega + ic$ , with  $0 < c < s$ , Eq.(16) is converted to

$$\theta(r,z) = 1 - \frac{1}{2\pi e^{(s-c)z}} \int_{-\infty}^{+\infty} \Phi(\omega + ic,1)g(\gamma)e^{-i\omega z} d\omega \quad (17)$$

where  $\gamma = \sqrt{(\omega + ic)^2 + s^2}$ . Various numerical inversion methods exist in the literature. Among them, the algorithm proposed by Gaver–Stehfest and the algorithm by Crump (based on Fourier series) are often applied. In the present analysis, numerical inversion by discrete Fourier transform is used. Based on this algorithm, the integral in Eq.(17) has been approximated by a discrete sum to obtain

$$\theta(r, z) = 1 - \frac{1}{2\pi e^{(s-c)z}} \sum_{n=-\infty}^{\infty} \Psi(\omega + ic) e^{-i\omega z} \Delta\omega \quad (18)$$

where  $\Delta\omega = \pi/T^*$  and  $T^*$  is the time period of the periodic function. It can be seen that by taking advantage of the symmetry property of  $\Psi(\omega + ic)$ , Eq.(18) can be reduced to following inversion formula:

$$\theta(r, z) = 1 - \frac{1}{T^* e^{(s-c)z}} \left[ \frac{\Psi_0}{2} + \text{Re} \sum_{n=1}^N \Psi_n e^{-in\pi z/T^*} \right] \quad (19)$$

Following Chu *et al.* [8], the parameter  $c$  in Eq.(19) has to be so chosen that  $(s-c)z$  does not exceed a specified value (usually 4 or 5). Expressions for the spectral coefficients  $\psi_0$  and  $\psi_n$  appearing in Eq.(19) are tabulated in the Appendix.

## Results and Discussion

Numerical values of dimensionless temperatures are obtained by evaluating Eq.(19), with  $Bi$ ,  $Pe$  and  $\delta$  as input parameters. The infinite series in Eq.(19) is summed up to  $N$  terms such that a convergence criterion of 0.001% change in value of  $\psi_n$  has been achieved, below which the summation series is truncated. Numerical computation of modified Bessel functions have been carried out by using the polynomial expressions [9] for both real and complex arguments. In this regard, it is informative to note that, the computation of  $f(\gamma)$  and  $g(\gamma)$  warrant special attention. Since the Bessel functions  $J_0$ ,  $I_1$  become infinite and  $K_0$ ,  $K_1$  become vanishingly small at higher values of arguments, they need to be evaluated with exponential scaling. The polynomial coefficients, once the exponential factor is removed, do not pose any data overflow/underflow problems. The temperature profiles are then plotted and depicted in graphical form.

Temperature profiles near the quench front are illustrated in Fig.3 for different Peclet numbers with  $Bi=10$ , where quench front temperature is found to increase with increase in Peclet number. With fixed material properties and dimensions,  $Pe$  and  $Bi$  represent the quench front velocity and

the heat transfer coefficient respectively. For a specified Biot number, quench front temperature increases with increase in quench front velocity. This is because of the fact that a higher relative velocity between the tube and the coolant allows less time for sufficient heat transfer to take place, resulting in a higher value of  $\theta_0$ . The above trend also reflects the fact that for the same

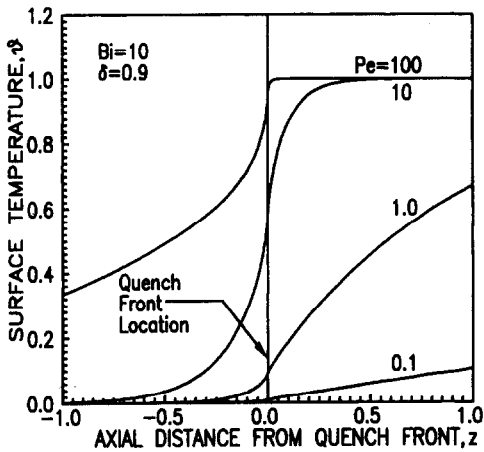


FIG.3  
Surface temperature distribution at  $r=1$ ,  
for various Peclet numbers.

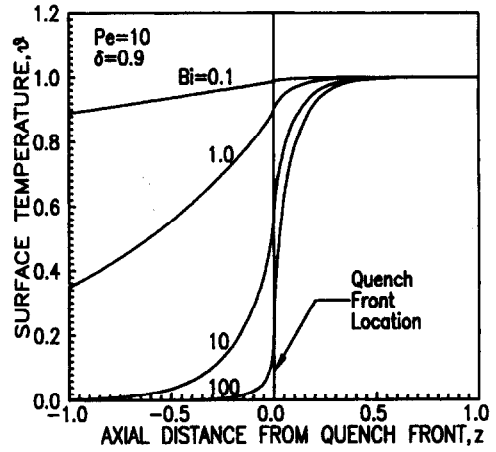


FIG.4  
Surface temperature distribution at  $r=1$ ,  
for various Biot numbers.

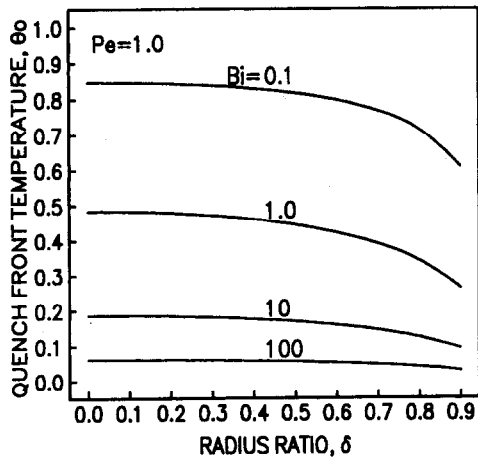


FIG.5  
Quench front temperature variation with  
radius ratio  $\delta$  and Biot number.

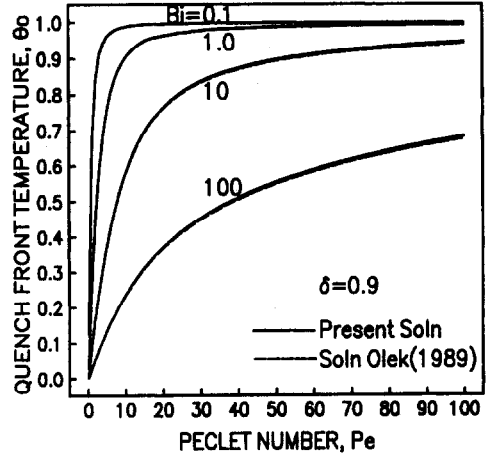


FIG.6  
Quench front temperature for various Biot  
and Peclet numbers for the tube ( $\delta=0.9$ ).

rewetting rate, an increasing tube thermal diffusivity tends to reduce  $\theta_0$ . Temperature profiles for different Biot numbers with  $Pe=10$  are shown in Fig.4, where quench front temperature is found to decrease with increase in  $Bi$ . A higher Biot number results in a higher heat transfer coefficient, which may cause to decrease  $\theta_0$ . Moreover, the temperature gradient at the quench front increases with increase in  $Pe$  in Fig.(3) and with increase in  $Bi$  in Fig.(4). This reveals the fact that axial conduction across the quench front becomes more significant at higher values of heat transfer coefficients and at higher quench front velocities.

The dependence of quench front temperature on radius ratio  $\delta$  is shown in Fig.(5), for fixed Biot and Peclet numbers. Here  $\theta_0$  is found to increase with decrease in radius ratio. The thickness of a tube increases with decrease in  $\delta$  and thereby its heat capacity also increases. Thus  $\theta_0$  is expected to increase with decrease in  $\delta$  owing to larger amount of initial heat content in a thicker tube. In the limiting case of a solid rod, where  $\delta$  is zero, quench front temperature assumes the maximum value. Finally the present solution has been compared with analytical solutions of [6] and a good agreement of data is observed in Fig.(6). Since number of terms  $N$  in the summation series (Eq.(19)) increases with increase in Biot number, the accumulated round-off errors (attributed to computation of the integrals involved in the spectral coefficients) may effect the present solution. Nevertheless, the present model may be beneficial in predicting the temperature distribution for an entire physical domain, whereas the aforementioned analytical solution is limited to quench front location only.

### **Conclusion**

A semi-analytical solution for the conduction controlled rewetting of an infinite tube has been obtained, employing the Wiener-Hopf technique and its numerical Fourier inversion by IDFT algorithm. The temperature distribution in the tube are plotted for a wide range of input model parameters. In particular, the parametric dependence of quench front temperature on various model parameters are shown in graphical form. In general, quench front temperature is found to increase with increase in Peclet number and with decrease in Biot number and radius ratio of the tube. It is felt that the present solution procedure, in principle, may be extended to more involved problems that include precursory cooling in the dry region or heat flux in the core in various other geometries.

## References

1. S. Olek, *Nuclear Engg. Design*, **108**, 315 (1988).
2. H. Levine, *Applied Scientific Research*, **39**, 261 (1982).
3. F. Castiglia, E. Olivery, S. Taibi & G. Vella, *8th Int. Heat Transf. Conf.*, San Francisco (1986).
4. S. Olek, *Int. Commun. Heat Mass Transfer*, **21**, 333 (1994).
5. D.V. Evans, *IMA J. Applied Mathematics*, **33**, 49 (1984).
6. S. Olek, *Int. Commun. Heat Mass Transfer*, **16**, 143 (1989).
7. S. H. Chan and W. Zhang, *ASME J. Heat Transfer*, **116**, 173 (1994).
8. H. S. Chu, C. I. Weng and C. K. Chen, *ASME J. Heat Transfer*, **105**, 307 (1983).
9. M. Abramowitz and I. A. Stegun, *Handbook of Mathematical Functions*, vol. 55, Dover Publications, New York (1968).

## Appendix

$$(a) \quad \Psi_0 = -\frac{1}{c-s} \frac{K_+(ic)}{K_+(is)} \left[ \frac{K(\alpha)-1}{K(\alpha)} \right] \left[ \frac{I_0(\gamma r)K_1(\gamma\delta) + I_1(\gamma\delta)K_0(\gamma r)}{I_0(\gamma)K_1(\gamma\delta) + I_1(\gamma\delta)K_0(\gamma)} \right]$$

$$K(\alpha) = 1 + \frac{Bi}{\gamma f(\gamma)}, \quad \text{with } \gamma = \sqrt{s^2 - c^2}$$

$$K_+(ic) = \exp \left[ \frac{1}{\pi} \int_0^{\pi/2} \ln \left( 1 + \frac{Bi}{\gamma f(\gamma)} \right) d\Omega \right], \quad \text{with } \gamma = \sqrt{c^2 \tan^2 \Omega + s^2}$$

$$K_+(is) = \exp \left[ \frac{1}{\pi} \int_0^{\pi/2} \ln \left( 1 + \frac{-Bi}{\gamma f(\gamma)} \right) d\Omega \right], \quad \text{with } \gamma = s \sec \Omega$$

$$(b) \quad \Psi_n = -\frac{i}{\omega_n + i(c-s)} \frac{K_+(\omega_n + ic)}{K_+(is)} \left[ \frac{K(\alpha)-1}{K(\alpha)} \right] \left[ \frac{I_0(\gamma r)K_1(\gamma\delta) + I_1(\gamma\delta)K_0(\gamma r)}{I_0(\gamma)K_1(\gamma\delta) + I_1(\gamma\delta)K_0(\gamma)} \right]$$

$$K(\alpha) = 1 + \frac{Bi}{\gamma f(\gamma)}, \quad \text{with } \gamma = \sqrt{(\omega_n + ic)^2 + s^2}, \quad \omega_n = \frac{n\pi}{T^*}$$

$$K_+(\omega_n + ic) = \exp(X - iY), \quad K(\tan \Omega) = 1 + \frac{Bi}{\gamma f(\gamma)}, \quad \text{with } \gamma = \sqrt{\tan^2 \Omega + s^2}$$

$$X = \frac{c}{2\pi} \int_{-\pi/2}^{+\pi/2} \frac{\ln K(\tan \Omega)}{[(\tan \Omega - \omega_n)^2 + c^{-2}]^2} \sec^2 \Omega d\Omega, \quad Y = \frac{1}{2\pi} \int_{-\pi/2}^{+\pi/2} \frac{(\tan \Omega - \omega_n) \ln K(\tan \Omega)}{[(\tan \Omega - \omega_n)^2 + c^{-2}]^2} \sec^2 \Omega d\Omega$$